



HAL
open science

Exfoliation and Delamination of $\text{Ti}_3\text{C}_2\text{T}_x$ MXene Prepared via Molten Salt Etching Route

Liyuan Liu, Metin Orbay, Sha Luo, Sandrine Duluard, Hui Shao, Justine Harmel, Patrick Rozier, Pierre-Louis Taberna, Patrice Simon

► **To cite this version:**

Liyuan Liu, Metin Orbay, Sha Luo, Sandrine Duluard, Hui Shao, et al.. Exfoliation and Delamination of $\text{Ti}_3\text{C}_2\text{T}_x$ MXene Prepared via Molten Salt Etching Route. ACS Nano, 2021, 16 (1), pp.111 - 118. 10.1021/acsnano.1c08498 . hal-03826847

HAL Id: hal-03826847

<https://hal.science/hal-03826847>

Submitted on 9 Nov 2022

HAL is a multi-disciplinary open access archive for the deposit and dissemination of scientific research documents, whether they are published or not. The documents may come from teaching and research institutions in France or abroad, or from public or private research centers.

L'archive ouverte pluridisciplinaire **HAL**, est destinée au dépôt et à la diffusion de documents scientifiques de niveau recherche, publiés ou non, émanant des établissements d'enseignement et de recherche français ou étrangers, des laboratoires publics ou privés.

Exfoliation and delamination of $\text{Ti}_3\text{C}_2\text{T}_x$ MXene prepared via molten salt etching route

Liyuan Liu^{1,2}, Metin Orbay^{1,2}, Sha Luo^{1,3}, Sandrine Duluard¹, Hui Shao^{1,2}, Justine Harmel^{1,2}, Patrick Rozier^{1,2}, Pierre-Louis Taberna^{1,2}, and Patrice Simon^{1,2}*

¹CIRIMAT, UMR CNRS 5085, Université Paul Sabatier Toulouse III, 118 route de Narbonne, 31062 Toulouse, France.

²RS2E, Réseau Français sur le Stockage Electrochimique de l'Energie, FR CNRS 3459, 80039 Amiens Cedex, France.

³State Key Laboratory of Applied Organic Chemistry (SKLAOC), The Key Laboratory of Catalytic Engineering of Gansu Province, College of Chemistry and Chemical Engineering, Lanzhou University, Lanzhou, Gansu, P. R. China

E-mail: (simon@chimie.ups-tlse.fr)

Keywords: (MXene, molten salt method, Li-ion batteries, exfoliation, delamination)

Abstract

MXenes are 2-Dimensional metal carbides or nitrides that are currently proposed in many applications thanks to their unique skills including high conductivity and accessible surface. Recently, a new synthetic route was proposed to prepare MXenes from the molten salt etching of precursors allowing for the preparation of MXene (denoted as MS-MXenes, for molten salt MXene) with tuned surface termination groups, resulting in improved electrochemical properties. However, further delamination of as-prepared multilayer MS-MXenes still remains a major challenge. Here, we report about the successful exfoliation of MS- $\text{Ti}_3\text{C}_2\text{T}_x$ via the

intercalation of organic molecule-TBAOH (Tetrabutylammonium hydroxide), followed by sonication to separate the layers. The treatment time could be adapted to tune the wetting behavior of the MS-Ti₃C₂T_x. As a result, self-supported Cl-terminated MXene film could be prepared for the first time by filtration. Finally, MS-Ti₃C₂T_x used as Li-ion battery anode could achieve high specific capacity of 225 mAh g⁻¹ at 1C rate together with an excellent rate capability of 95 mAh g⁻¹ at 167C. These results also show that tuning of the surface chemistry of MXene is of key importance for enhancing their electrochemical properties, providing the basis for a new generation of high-power batteries.

1. Introduction

The discovery of two-dimensional (2D) transition metal carbides or carbonitrides in 2011, termed as MXenes, has attracted wide attention from the research community due to its great potential applications in various fields¹⁻³. MXenes are conventionally prepared by selective etching in F-containing aqueous electrolyte of atomically thin A layer elements from MAX phase precursors, where M stands for an early transition metal (Sc, Ti, V, Nb, Cr, etc.), A represents an element from group 13-16 (Al, Si, etc.) and X is carbon and/or nitrogen². The general formula of MXenes is M_{n+1}X_nT_x (n=1-3) where T denotes surface groups such as OH, O, and/or F groups^{1,4-6}. The surface functional groups of MXenes not only affect the thermodynamic stability and optical properties, but also the electronic (including band structure, work function) and electrochemical performance⁷. Although no method has been found so far to finely tune the types of surface functional groups, those surface terminations are highly dependent on the synthetic route and post-synthesis treatment^{8,9}.

Until recently, aqueous solutions containing fluoride ions remained the mainstream method to etch A-layer of MAX phase to prepare MXenes. Etching electrolytes such as hydrofluoric acid (HF²) or fluoride-based compounds (LiF+HCl¹⁰, (NH₄)HF₂¹¹) are used, which results in -F,-

OH, and -O surface terminated MXene (hereinafter termed as HF-MXene). All the etching mechanisms of the above methods involved the use/formation of hazardous HF solution. It then appears particularly important to find alternative, non-hazardous synthesis routes to achieve scalable preparation of MXenes. Recently, Li et al. reported about the synthesis of Zn-based MAX phase and surface F-free, Cl-terminated MXenes by reaction of MAX phase and Lewis acidic molten salt at 550 °C via a replacement reaction mechanism¹². Following this pioneering work, the synthesis of MS-MXenes was extended to a wide range of elements for the A-site of the MAX precursors (Zn, Al, Si, Ga) and Lewis acid melt composition¹³⁻¹⁵. The influence of the nature of the surface functional groups on the electrochemical performance of MS-MXene was also studied¹³. Used as Li-ion battery anode, MS- $\text{Ti}_3\text{C}_2\text{T}_x$ delivered a Li^+ storage capacity up to 200 mAh g^{-1} in 1 M LiPF_6 carbonate-based electrolyte with good power performance (~100 mAh. g^{-1} at 60C). However, the rate performance was limited by the difficulty in exfoliating / delaminating further the prepared multi-layered MS-MXene particles as the result of the change of synthesis route and surface groups.

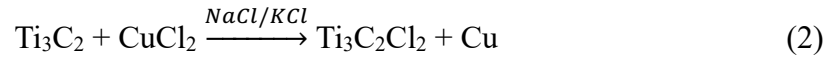
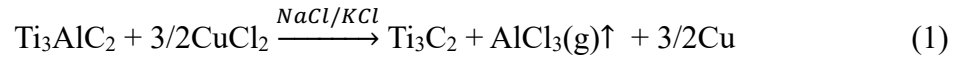
Over the past few years, important research efforts have been put in HF-MXene delamination to improve their electrochemical performance compared to their multilayered counterparts^{16,17}. Several organic molecules such as dimethyl sulfoxide (DMSO)¹⁶, isopropylamine¹⁸ or tetrabutylammonium hydroxide (TBAOH)¹⁹ have been reported as effective intercalants for efficient HF-MXenes delamination¹⁷.

In this work, we propose to further exfoliate MS-MXene by intercalation of Tetrabutylammonium tetrafluoroborate (TBAOH) organic molecule, followed by sonication to separate the layers. The electrochemical behavior of MS- $\text{Ti}_3\text{C}_2\text{T}_x$ used as Li-ion battery anode before and after further exfoliation was compared, as well as the hydrophilic properties of the $\text{Ti}_3\text{C}_2\text{T}_x$ / electrolyte interface. In addition, delaminated MS- $\text{Ti}_3\text{C}_2\text{T}_x$ MXene could be successfully prepared by extending the surfactant treatment and sonification time in TMAOH.

2. Results and discussion

2.1. Materials Characterizations

Figure 1a shows a sketch of the reaction between Ti_3AlC_2 and CuCl_2 at 680°C during Ti_3C_2 MXene synthesis; the reactions are listed below:



CuCl_2 together with NaCl/KCl turned to a molten state at the reaction temperature. Al layer in Ti_3AlC_2 is oxidized into Al^{3+} by concomitant reduction of the Lewis acid Cu^{2+} into Cu onto the MXene surface; further AlCl_3 gas is formed, which can act as an effective agent to expand the MXene layer (equation 1) ¹². Excess of Cu^{2+} also partially reacts with the exposed Ti atoms from Ti_3C_2 to form metallic Cu, while charge compensation is ensured by Cl^- anions reacting to form $\text{Ti}_3\text{C}_2\text{Cl}_2$ (equation 2) ¹². The formation mechanism of $\text{Ti}_3\text{C}_2\text{Cl}_2$ from Ti_3AlC_2 is analogous to that of chemical etching of Ti_3AlC_2 in HF solution, where Cu^{2+} and Cl^- act as H^+ and F^- , respectively ². As-prepared powders of $\text{Ti}_3\text{C}_2\text{Cl}_2$ were further immersed in ammonium persulfate (APS) oxidizing solution to remove Cu particles from the $\text{Ti}_3\text{C}_2\text{Cl}_2$ MXene surface, which also results in the addition of O-based surface groups. This final material prepared from this molten salt route will be noted as MS- $\text{Ti}_3\text{C}_2\text{T}_x$ MXene, where T_x stands for O and Cl surface groups; under these experimental conditions, no $-\text{OH}$ or $-\text{F}$ surface termination is present on MS-MXene surface ¹³.

For conventional HF-MXenes, one of the most widely applied methods for delamination is to intercalate DMSO solvent followed by sonication ¹⁷, thanks to matching the surface energy between DMSO and HF-MXene; however, this method failed to produce delaminated MS- $\text{Ti}_3\text{C}_2\text{T}_x$. As shown in Figure S1, SEM image of DMSO-treated MS- $\text{Ti}_3\text{C}_2\text{T}_x$ show thick, multi-layers MS-MXene flakes, and precipitation in the solution is observed after just a couple of hours. After APS washing, the pH of MS- $\text{Ti}_3\text{C}_2\text{T}_x$ in deionized water is 3.9, indicating the

release of protons from MS-Ti₃C₂T_x MXene in the electrolyte. In addition, a small number of K-ions coming from the MS precursor still remain on the MXene surface (see Table S1). After the addition of TBAOH into the MS-Ti₃C₂T_x suspension, the pH gradient between the acidic MS-MXene and alkaline TBAOH electrolyte results in ion exchange between the bulky tetraalkylammonium ions (TBA⁺) and cations (protons and K-ions), leading to MXene structure swelling. After sonication to promote exfoliation, TBAOH-treated MS-Ti₃C₂T_x were centrifuged at 3500 rpm for 30 mins to eliminate the sediment. Figure 1b shows the pristine and TBAOH-treated MS-Ti₃C₂T_x after centrifugation followed by sonication. For pristine MS-Ti₃C₂T_x, the precipitation occurs after only 2 hours while the suspension of TBAOH treated MS-MXene is still stable after 2 weeks (see Figure S2). By shining a laser beam into the suspension of TBAOH treated MS-MXene, a clear Tyndall effect can be observed as shown in Figure 1d, thereby confirming the existence of colloidal suspension¹⁸. Differently from pristine MS-MXene, the TBAOH-treated MS-MXene material can form a film after filtration as shown in Figure 1c; however, the film is brittle with poor mechanical properties, differently from HF-MXene after delamination¹⁰. MS-Ti₃C₂T_x has also been treated with 1M NaOH and TEAOH by following the same procedure, but no stable suspension could be obtained (Figure S3). Large TBA⁺ cation results in improving the stability of suspension, assumed to be linked with a decrease in the flake thickness and improved exfoliation of the MS-MXene.

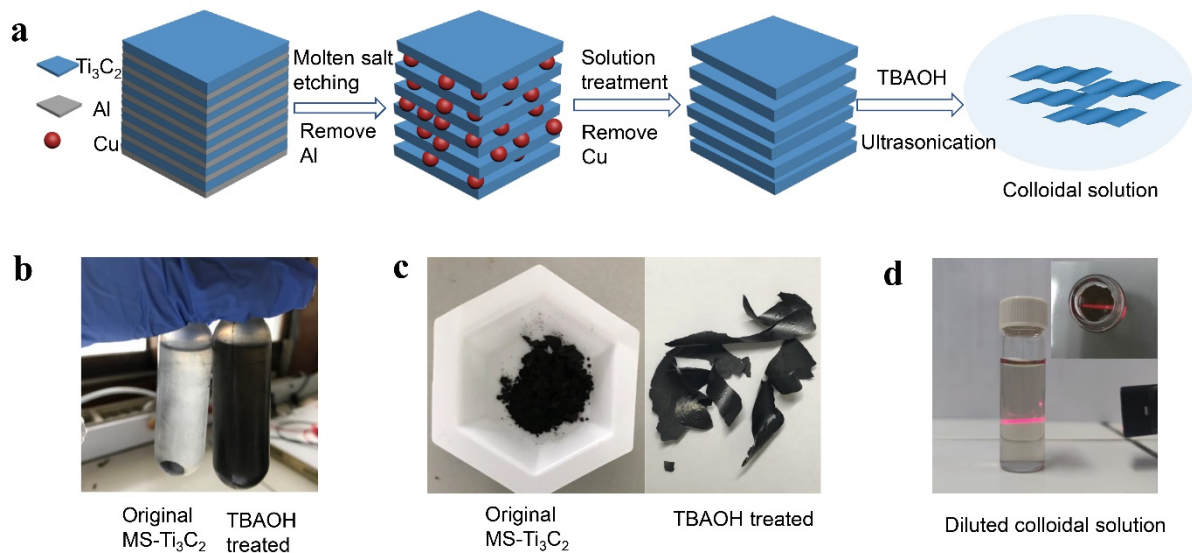


Figure 1: Schematic and realistic views of the molten salt synthesis method and exfoliation process. (a) Schematic representation of synthesis and exfoliation of MXene prepared via Lewis acidic etching route. Pristine MS-Ti₃C₂T_x before (left) and after (right) TBAOH treatment after (b) centrifugation at 3500 rpm for 30 mins and (c) collected by filtration. (d) shows the Tyndall effect for nano flakes dispersed in water after TBAOH treatment.

Figure 2a shows the XRD patterns of the MAX phase precursor (black plot), the MXene after removal from the molten salt bath (red plot), after washing in ammonium persulfate solution (APS) to remove Cu (blue plot), and the MXene after TBAOH exfoliation treatment (green). Right after synthesis (Figure 2a, red plot), most of the diffraction peaks corresponding to the pristine Ti₃AlC₂ MAX precursor disappeared, leaving (001) peaks as well as several broad and low-intensity peaks in the 2θ range from 5° to 80°. These features indicate the successful etching of Al-layer from Ti₃AlC₂ into layered Ti₃C₂. Additionally, the shift of Ti₃C₂ (002) diffraction peaks from 2θ = 10.13° to 8.07° (±0.02°) indicates an expansion of the interlayer distance from 8.8 to 10.98 Å (±0.03 Å). The newly formed sharp and intense peaks centered at 2θ angles of 43.29°, 50.43°, and 74.13° can be identified as metallic Cu. XRD pattern after washing with APS ((NH₄)₂S₂O₈) solution only shows (001) peaks (Figure 2a, blue plot) as a

result of Cu removal. After TBAOH treatment and freeze drying, the main peaks of MS-Ti₃C₂T_x in the XRD pattern (Figure 2a, green plot) still remain, which evidences Ti₃C₂T_x. The low intensity of (002) and (004) peaks reveals that freeze-dried TBAOH treated MS-MXene flakes sit in a different orientation. In addition, both (002) and (004) peaks slightly shift from 8.0° to 7.6° and 16.0° to 15.2° respectively for (002) and (004) peaks. This indicates a slight expansion of the MS-MXene structure following intercalation of TBA cation, from 18.5 Å (neat) to 22.0 Å (after TBAOH treatment). At the same time, slight peak broadening is observed, indicating a smaller flake size²⁰. Differently from the accordion-like multi-layered morphology of original MS-Ti₃C₂T_x (Figure 2b), parallel restacked layered morphology (Figure 2c) was observed after TBAOH treatment and filtration, further confirmed by parallel stacking as shown in the cross-section image (Figure S4). TEM image (Figure 2d) shows transparent Ti₃C₂T_x sheets with well-defined and clean edges, with the lateral size around 600 nm. Selected area electron diffraction pattern (SAED) (Figure 2e), shows sharp reflections indexed with hexagonal crystal system indicating that the TBAOH treatment does not alter the crystallinity of the Ti₃C₂T_x nanosheets²¹. The high-resolution TEM (HRTEM) image in Figure 2f confirms the thickness is around 2.05 nm, corresponding to ~2 layers considering the thickness of monolayer (~1.03 nm)^{22,23}. These samples with expanded interlayer distance will be further termed as e-MS-Ti₃C₂T_x. Zeta-potential (ζ) measurements of MS-Ti₃C₂T_x suspensions before and after TBAOH treatment have been made in water at different pH. to determine the surface charge and the fundamental interaction between the particles. As shown in Figure 2g, a negative ζ was measured in a pH range from 2.9 to 10.2 varied from 0 to -67 mV. The maximum zeta potential (absolute value) is almost twice compared to DMSO-treated HF-Ti₃C₂T_x¹⁶, but similar to TBAOH treated HF-Ti₃CNT_x¹⁹. The isoelectric point is located at pH 2.9, which is far away from the pH of e-MS-Ti₃C₂T_x (pH=7.6) in water. The strong electrostatic repulsion between highly negatively charged e-Ti₃C₂T_x nanosheets results in stable colloidal suspension by limiting aggregation, such as previously observed for DMSO-treated HF-MXene¹⁶. Differently from e-MS-Ti₃C₂T_x,

the zeta potential of pristine MS-Ti₃C₂T_x is nearly 0 mV as a function of pH (Figure 2h), as the result of the instability of the pristine MS-Ti₃C₂T_x suspension after a couple of hours. Finally, the determination of the particle size (Figure 2i) shows, after TBAOH treatment and sonication, a size range from 200 nm to 1000 nm with the distribution of peak positions at 600 nm which corresponds well with the TEM results (Figure 2d).

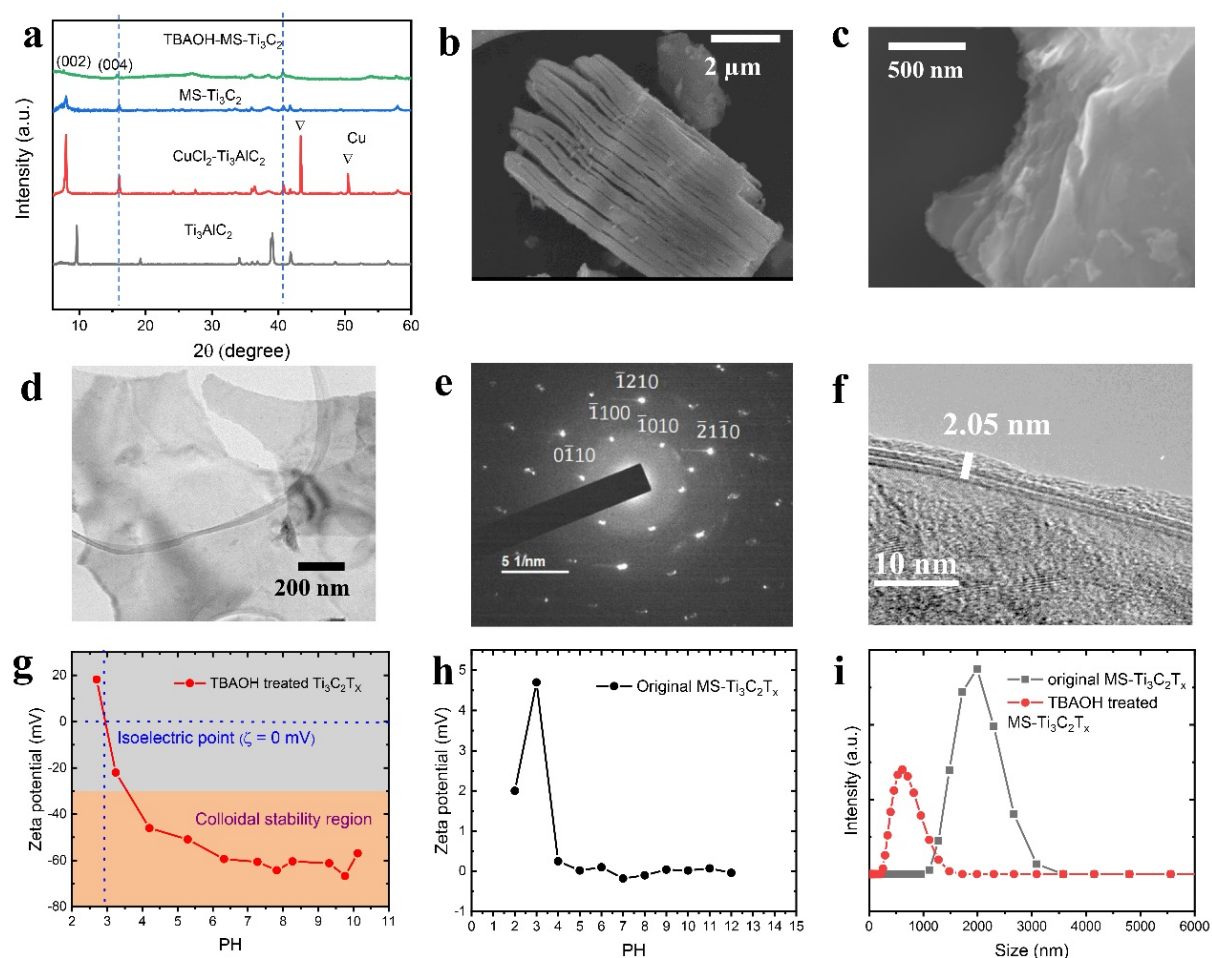


Figure 2: Material characterization of e-MS-Ti₃C₂T_x. (a) XRD patterns of pristine Ti₃AlC₂ before (black line) and after (red line) reaction with CuCl₂, multi-layered MS-Ti₃C₂T_x (blue line) and e-MS-Ti₃C₂T_x (green line) TBAOH treatment. SEM graph of (b) MS-Ti₃C₂T_x MXene and (c) e-MS-Ti₃C₂T_x (collected by filtration). (d) TEM graph of e-MS-Ti₃C₂T_x. (e) Selected area electron diffraction (SAED) pattern and (f) HRTEM image of e-MS-Ti₃C₂T_x. Zeta potentials of (g) e-MS-Ti₃C₂T_x and (h) multi-layered MS-Ti₃C₂T_x. (i) Mean size of multi-layered MS-Ti₃C₂T_x (grey line) and e-MS-Ti₃C₂T_x (red line) in DI water.

2.2. Electrochemical Characterizations

A series of electrochemical characterizations were performed to evaluate the electrochemical performance of freeze-dried e-MS-Ti₃C₂T_x. Figure 3a shows the initial two CV cycles recorded at 1 mV s⁻¹ in LP30 electrolyte (1 M LiPF₆ in ethylene carbonate/dimethyl carbonate with 1:1 volume ratio). During the first cycle, an irreversible capacity loss is observed upon reduction (lithiation) due to the formation of the solid electrolyte interphase (SEI) layer²⁴. The SEI layer formation at the first cycle decreases the coulombic efficiency down to 36%, as a result of the increased electrochemical surface area. Although we did not focus on that specific point, the coulombic efficiency at the first cycle could be improved by post-annealing treatment for instance²⁵. In the subsequent cycle, CV shows a mirror-like shape with no redox peak during Li intercalation/deintercalation reactions, similarly to what we previously observed for pristine MS-Ti₃C₂T_x (Figure S5a, see also¹³). In Figure 3b, an almost constant current was observed during the oxidation process from 1 mV s⁻¹ to 200 mV s⁻¹ in a potential range between 0.2 and 2.0 V versus Li⁺/Li, indicating a reversible behavior for the freeze-dried e-MS-Ti₃C₂T_x. The discharge capacity of freeze-dried e-MS-Ti₃C₂T_x is 225 and 95 mA h g⁻¹ at current densities of 0.2 and 16 A g⁻¹, respectively (Figure 3c), corresponding to an impressive ~42% capacity retention after 80 times increases of current density. Comparatively, the discharge capacities of pristine MS-Ti₃C₂T_x can only reach 205 and 25 mA h g⁻¹ at current densities of 0.2 and 16 A g⁻¹, respectively (Figure S5c). Figure 3d compares the specific capacity of MS-Ti₃C₂T_x before and after TBAOH treatment at different C-rates calculated from the galvanostatic charge-discharge profiles (Figures 3c and S5c), where both electrodes have similar weight loading of 1.1 mg.cm⁻². The capacity retention of e-MS-Ti₃C₂T_x reaches 42% from 0.2 to 16 A g⁻¹, while pristine MS-Ti₃C₂T_x with similar weight loading shows only 15% retention in the same current range due to slow kinetic even at 20 mV s⁻¹. Those numbers evidence the higher power

capability of the e-MS-Ti₃C₂T_x which can be explained by the improved electrochemically accessible specific surface area of e-MS-Ti₃C₂T_x and faster ion transport²⁶. EDS analysis of the e-MS-Ti₃C₂T_x show that the main effect of the TBAOH treatment is the -O content increases (see Table S1), indicating the possible -O group addition due to the dissolved oxygen during the 6h sonification process. These results agree well with the result of DFT stimulations showing that O-terminated Ti₃C₂ MXene exhibits the highest theoretical Li ion storage capacity²⁷. The cycling stability of the e-MS-Ti₃C₂T_x has also been test at a current density of 4 A g⁻¹. As shown in Figure S6, it reveals that the capacity can retain about 85 mA h g⁻¹ over 2000 cycles, gives a capacity retention of 72%. Moreover, the electrochemical performance of TBAOH treated MXene is also strongly affected by the drying methods²⁸. While oven-dried (80 °C for 12 hours) e-MS-Ti₃C₂T_x have a similar electrochemical signature as freeze-dried one (Figure S7a), gravimetric capacity and power performance are strongly affected (Figures S7b and c) as a result of limited Li-ion transport in the electrode structure due to the stacking of oven-dried e-Ti₃C₂T_x layers²⁸, supported by the presence of sharp (002) and (004) peaks in the XRD pattern in Figure S8. In addition, the electrochemical performance of freeze-dried MS-Ti₃C₂T_x has also been evaluated to evidence the significance of TBAOH treatment. As shown in Figure S9, without TBAOH treatment, freeze-dried MS-Ti₃C₂T_x shows similar capacity (180 mAh g⁻¹) and low power capability as observed for oven-dried MS-Ti₃C₂T_x.

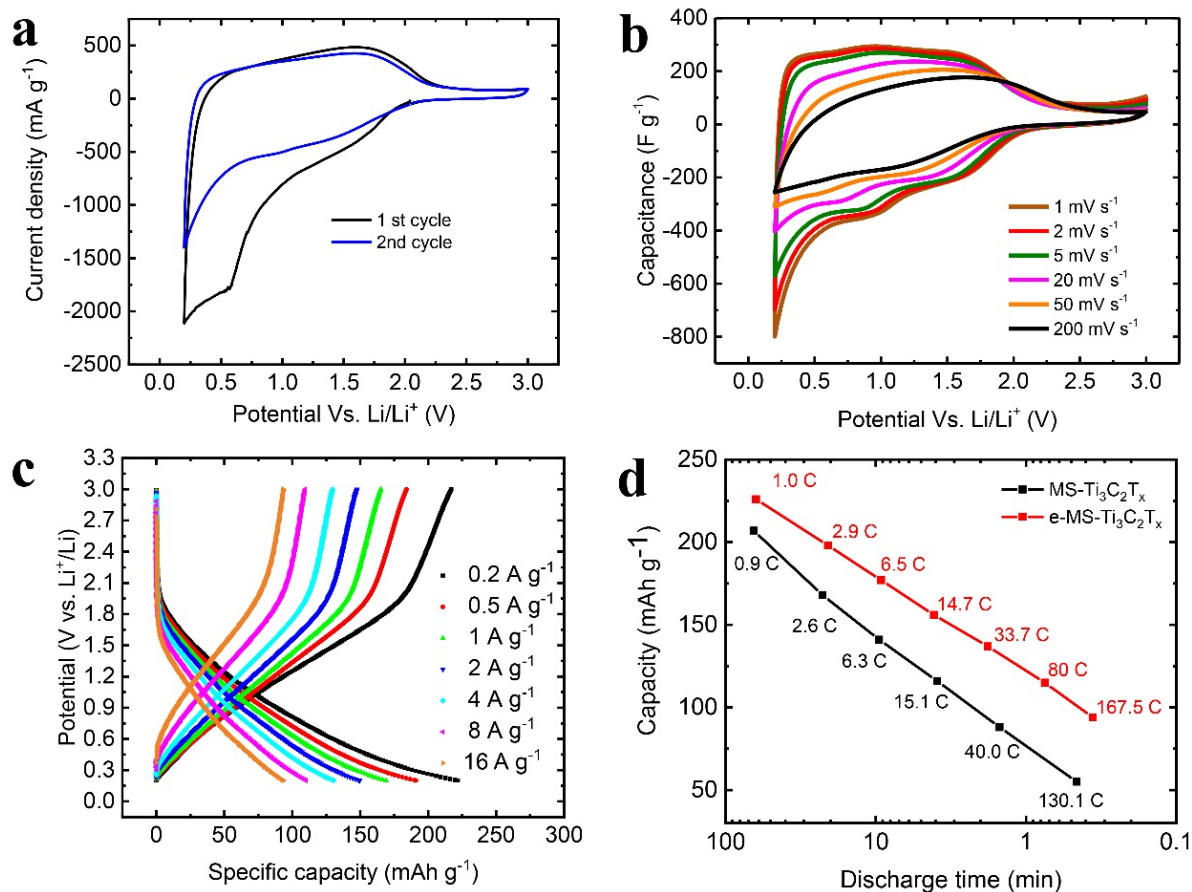


Figure 3: Electrochemical characterization in 1 M LiPF₆ in ethylene carbonate/dimethyl carbonate electrolyte of e-MS-Ti₃C₂T_x with a mass loading of 1.1 mg.cm⁻². (a) Initial first three CV cycles recorded at 1 mV s⁻¹ (b) CVs recorded at various potential scan rates from 1 to 200 mV s⁻¹. (c) Galvanostatic charge discharge (GCD) curves recorded at various current density from 0.2 A g⁻¹ to 16 A g⁻¹. (d) Discharge time and capacity values of a multi-layered before (black line) and after (red line) TBAOH treatment from 0.2 A g⁻¹ (1C) to 16 A g⁻¹ (167.5C).

2.3. Interface Modification of MS-Ti₃C₂T_x

Differently from the hydrophilic HF-MXene²⁸, pristine MS-MXene has a hydrophobic surface due to the absence of -OH group on the surface. To further characterize the change of surface properties, water contact angle measurements were performed on MS-MXene electrode film (prepared by mixing 80 wt% of MXenes powders together with 15 wt% of carbon black and 5 wt% of PTFE binder) before and after TBAOH treatment. As shown in Figure 4a, different

TBAOH treatment times lead to distinct wetting behavior of MS-Ti₃C₂T_x. Pristine MS-Ti₃C₂T_x film presents a hydrophobic nature with a water contact angle of 136°, whereas the MS-Ti₃C₂T_x samples after TBAOH treatment show a decreasing contact angle with the TBAOH treatment time (see Figure 4a). The WCA values were 118°, 95°, and 43° for 12, 24 and 72h treatment time, respectively, indicating that the hydrophilicity increases with longer TBAOH treatment time. According to the report of Liu et al.³⁰, the hydrophilicity of MXene materials can be improved by introducing oxygen-containing polar groups. In the present case, the immersion in strong TBAOH base may result in slow surface oxidation of MXene surface into hydroxyl groups under a prolonged sonication process, possibly by dissolved oxygen²⁹. To further understand the evolution of MS-MXene in TBAOH solution, TEM observations and electrochemical measurements were successively performed on the MS-Ti₃C₂T_x after TBAOH treatment for 24h and 72h. As shown in Figure S10, some black dots were present on both basal and edge planes of MS-Ti₃C₂T_x sheets after 24h, and large defects and nanoparticles of about 50 nm diameter can be observed after 72h. Moreover, a new peak at 25.2° corresponding to anatase TiO₂ can be observed in the XRD patterns (see Figure S11a) of MS-Ti₃C₂T_x after 72h treatment in TBAOH solution, indicating that Ti₃C₂T_x slowly oxidized into TiO₂ (PDF#00-021-1272)^{9,31}. This is supported by the electrochemical signature of MS-Ti₃C₂T_x, where broad cathodic peak at 1.2 V and anodic peak at 2.1 V observed with increasing the treatment time (Figure S11b) could be attributed to the (de)lithiation behavior of TiO₂⁹.

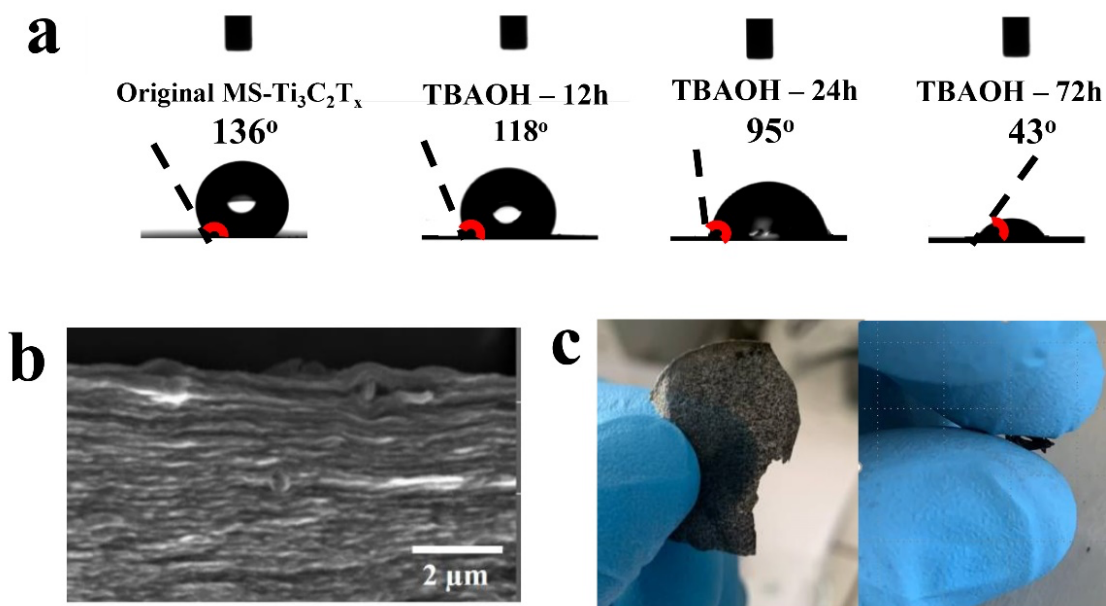


Figure 4: Evolution of MS-Ti₃C₂T_x in TBAOH and TMAOH. (a) Water contact angle of MS-Ti₃C₂T_x treated by TBAOH for 0h, 12 h, 24h, and 72h, respectively. (b) SEM image of MS-Ti₃C₂T_x MXene after TMAOH treatment for 72 hours, followed by 18 hours bath sonification and selection at 7000 rpm. (c) Photo showing the flexibility of the filtrated TMAOH treated MS-MXene after selection.

It was reported that hydroxyl groups play a significant role in the delamination of MXene³². Therefore, a more hydrophilic TMAOH, due to the shorter chain size, has been chosen to treat MS-Ti₃C₂T_x for 72 h, followed by 18 h bath sonification and selection by centrifugation at 7000 rpm. As shown in Figures 4b and 4c, free-standing Ti₃C₂T_x paper could be prepared by filtration of the suspension onto a porous membrane. To the best of our knowledge, this is the first report of MS-MXene self-supported thin film. The water contact angle of the above free-standing film is measured to be 24.2° (see Figure S12), which evidences its more hydrophilic surface. However, the filtered electrode shows poor electrochemical performance in 1 M LiPF₆ in ethylene carbonate/dimethyl carbonate electrolyte (Figure S13) as a result of hydrophilic

surface groups and compact layered structure which limits full access of the electrolyte ions between the MXene layers.

3. Conclusions

In this paper, TBAOH was selected as a solvent for the exfoliation of MS-Ti₃C₂T_x. During the process, ion exchange between the bulky tetraalkylammonium ions (TBA⁺) and cations (protons and K-ions) is assumed to allow bulky TBA⁺ cation to access the interlayer space, resulting in further exfoliation from multi- to few-layer MXene. The TBAOH treated MS-Ti₃C₂T_x nanosheet suspension was found to be stable for two weeks, without apparent precipitation. When TBAOH-treated MS-Ti₃C₂T_x was tested as anode material in Li-ion battery, a high specific capacity of 225 mAh g⁻¹ at 1C and excellent rate capability of 95 mAh g⁻¹ at 167C could be achieved, indicating improved electrochemical performance versus multilayered (pristine) MS-Ti₃C₂T_x. Interestingly, TBAOH treatment resulted in the change of the wettability of MS-MXene, as evidenced from the decrease of contact angle with the duration of TBAOH treatment time. Moreover, self-supported Cl-terminated MXene film could be prepared for the first time by filtration.

4. Experimental

4.1. Preparation of MS-MXenes

Ti₃AlC₂ was used as the MAX phase precursor, and CuCl₂ (Sigma-Aldrich, CAS # 7447-39-4), NaCl (Sigma-Aldrich, CAS # 7647-14-5) and KCl (Sigma-Aldrich, CAS # 7447-40-7) were selected as the molten salt. In a typical procedure, Ti₃AlC₂ was mixed with molten salt according to the following ratio (Ti₃AlC₂:CuCl₂:NaCl:KCl = 1:3:2:2 in molar ratio) and grinded well for 10 minutes in air to make sure the mixture was homogeneous. Then the mixture was heated to 680 °C at a heating ramp of 4°C/ min under flowing argon in a tube furnace for 24 h.

The resulting reddish-brown products were washed using deionized water and collected by vacuum filtration with a porous anodic aluminum oxide membrane filter (47 mm diameter, 0.2 mm pore size, Whatman Anodisc, Maidstone, UK). Afterward, APS ((NH₄)₂S₂O₈, Sigma-Aldrich, CAS # 7727-54-0) solution was prepared and added inside to further dissolve the residual Cu. Finally, the above products were collected by vacuum filtration after cleaning by deionized water and then dried in a vacuum oven at 80 °C overnight.

4.2. Exfoliation and delamination of MS-MXenes

0.2 g of MS-Ti₃C₂T_x were added to 5 mL of aqueous solution of Tetrabutylammonium hydroxide (TBAOH, 40%) and 10 ml deionized water under Ar gas, and kept overnight under stirring at 40 °C in water bath. The obtained colloidal MXene suspension was then centrifuged at 15300 rpm and 9000 rpm with a large excess of water to totally separate the intercalated powder from the liquid TBAOH. Deionized water was subsequently added to the residue in a weight ratio of MXene to the water of 1:500. Ultrasonication of the bath was carried out for 6 h at low temperature (ice) to limit oxidation. Then, the TBAOH treated MS-MXenes were centrifuged at 3500 rpm for 30 mins to eliminate the sediment. After the elimination of the precipitate, the MXene was dried via vacuum freeze-drying for 4 days. For delamination, the MS-Ti₃C₂T_x MXene was left in TMAOH for 72 h, in which 18 h were dedicated to sonication in an iced bath to avoid oxidation. The sonication was accomplished as a step-by-step process (6 h each day) and stored inside the freezer during the rest of the time. Following the sonication process, the solution was centrifuged at 15300 rpm for 15 min to precipitate all particles and the above TMAOH solution was removed by using a pipette. Finally, the delaminated MS-MXene were centrifuged at 7000 rpm for 8 mins to eliminate the sediment. After the elimination of the precipitate, the delaminated MXene was collected by vacuum filtration.

4.3. Physical characterizations

X-ray diffraction (XRD) data was collected by a D4 ENDEAVOR X-ray diffractometer (Bruker, Germany) equipped with $\text{CuK}\alpha$ radiation ($\lambda = 0.154$ nm). The morphology of the MXenes was observed with a Scanning Electron Microscope (SEM) JSM 7100F (JEOL, Japan). Transmission Electron Microscopy (TEM) and High-Resolution Transmission Electron Microscopy (HTEM) images were performed using a JEM-2100 F microscope working at an acceleration voltage of 200 kV. The zeta potential was measured using a Zetasizer Nano ZS90 (Malvern Instruments Ltd., UK, England). The pH for the solutions of MXenes in deionized (DI) water was adjusted using HCl and NaOH. At each pH value, ten measurements were collected for the zeta potential and the mean value was reported. The water contact angle (WCA) was measured via a contact angle meter (DSA30 Drop Shape Analyzer from Kruss).

4.4. Electrochemical measurements

MXene powders were processed into free-standing electrode films by mixing 80wt% of MXenes powders together with 15wt% of carbon black and 5wt% of PTFE binder; followed by vacuum drying for one day. The electrode mass loading was 1.1 mg cm^{-2} . Lithium metal foils were used as both counter and reference electrodes, and Cu disk as working electrode current collector. The electrolyte was a commercial solution of LP30 (1 M LiPF_6 in ethylene carbonate/dimethyl carbonate with 1:1 volume ratio) and two layers of 260 μm -thick porous glass fibers (Whatman GF/A) were used as the separator. Two-electrode Swagelok cells were assembled in an argon-filled glove box (moisture < 0.1 ppm, oxygen < 0.1 ppm) to perform electrochemical measurements.

Cyclic voltammetry, electrochemical impedance spectroscopy and galvanostatic cycling were performed using a VMP3 potentiostat (Biologic, France). Cyclic voltammetry and Galvanostatic cycling was carried out within a potential range from 0.2 to 3V vs. Li/Li^+ .

Electrochemical impedance spectroscopy (EIS) was performed at open circuit potential with a 10 mV amplitude between 10 mHz and 200 kHz.

AUTHOR INFORMATION

Corresponding Author

Patrice Simon - CIRIMAT, UMR CNRS 5085, Université Paul Sabatier Toulouse III, 118 route de Narbonne, 31062 Toulouse, France; RS2E, Réseau Français sur le Stockage Electrochimique de l'Energie, FR CNRS 3459, 80039 Amiens Cedex, France.

E-mail: simon@chimie.ups-tlse.fr

Authors

Liyuan Liu - CIRIMAT, UMR CNRS 5085, Université Paul Sabatier Toulouse III, 118 route de Narbonne, 31062 Toulouse, France; RS2E, Réseau Français sur le Stockage Electrochimique de l'Energie, FR CNRS 3459, 80039 Amiens Cedex, France.

Metin Orbay - CIRIMAT, UMR CNRS 5085, Université Paul Sabatier Toulouse III, 118 route de Narbonne, 31062 Toulouse, France; RS2E, Réseau Français sur le Stockage Electrochimique de l'Energie, FR CNRS 3459, 80039 Amiens Cedex, France.

Sha Luo - CIRIMAT, UMR CNRS 5085, Université Paul Sabatier Toulouse III, 118 route de Narbonne, 31062 Toulouse, France; State Key Laboratory of Applied Organic Chemistry (SKLAOC), The Key Laboratory of Catalytic Engineering of Gansu Province, College of Chemistry and Chemical Engineering, Lanzhou University, Lanzhou, Gansu, P. R. China.

Sandrine Duluard - CIRIMAT, UMR CNRS 5085, Université Paul Sabatier Toulouse III, 118 route de Narbonne, 31062 Toulouse, France.

Hui Shao - CIRIMAT, UMR CNRS 5085, Université Paul Sabatier Toulouse III, 118 route de Narbonne, 31062 Toulouse, France; RS2E, Réseau Français sur le Stockage Electrochimique de l'Energie, FR CNRS 3459, 80039 Amiens Cedex, France.

Justine Harmel - CIRIMAT, UMR CNRS 5085, Université Paul Sabatier Toulouse III, 118 route de Narbonne, 31062 Toulouse, France; RS2E, Réseau Français sur le Stockage Electrochimique de l'Energie, FR CNRS 3459, 80039 Amiens Cedex, France.

Patrick Rozier - CIRIMAT, UMR CNRS 5085, Université Paul Sabatier Toulouse III, 118 route de Narbonne, 31062 Toulouse, France; RS2E, Réseau Français sur le Stockage Electrochimique de l'Energie, FR CNRS 3459, 80039 Amiens Cedex, France.

Pierre-Louis Taberna - CIRIMAT, UMR CNRS 5085, Université Paul Sabatier Toulouse III, 118 route de Narbonne, 31062 Toulouse, France; RS2E, Réseau Français sur le Stockage Electrochimique de l'Energie, FR CNRS 3459, 80039 Amiens Cedex, France.

Notes

The authors declare no competing financial interest.

Acknowledgements

L. Liu was supported by ERC Synergy Grant MoMa-Stor #951513. P. Simon and P.L. Taberna acknowledge the support from Agence Nationale de la Recherche (Labex Store-ex) and ERC Synergy Grant MoMa-Stor #951513. Metin Orbay was supported by the Mundus plus “MESC” Master programme of the European Commission.

Received: ((will be filled in by the editorial staff))
Revised: ((will be filled in by the editorial staff))
Published online: ((will be filled in by the editorial staff))

Reference

- (1) Lukatskaya, M. R.; Mashtalir, O.; Ren, C. E.; Dall'Agnese, Y.; Rozier, P.; Taberna, P. L.; Naguib, M.; Simon, P.; Barsoum, M. W.; Gogotsi, Y. Cation Intercalation and High

- Volumetric Capacitance of Two-Dimensional Titanium Carbide. *Science* (80-.). **2013**, *341* (6153), 1502–1505.
- (2) Naguib, M.; Kurtoglu, M.; Presser, V.; Lu, J.; Niu, J.; Heon, M.; Hultman, L.; Gogotsi, Y.; Barsoum, M. W. Two-Dimensional Nanocrystals Produced by Exfoliation of Ti₃AlC₂. *Adv. Mater.* **2011**, *23* (37), 4248–4253.
 - (3) Wang, X.; Mathis, T. S.; Li, K.; Lin, Z.; Vlcek, L.; Torita, T.; Osti, N. C.; Hatter, C.; Urbankowski, P.; Sarycheva, A.; et al. Influences from Solvents on Charge Storage in Titanium Carbide MXenes. *Nat. Energy* **2019**, *4* (3), 241–248.
 - (4) Beda, A.; Taberna, P. L.; Simon, P.; Matei Ghimbeu, C. Hard Carbons Derived from Green Phenolic Resins for Na-Ion Batteries. *Carbon N. Y.* **2018**, *139*, 248–257.
 - (5) Lukatskaya, M. R.; Kota, S.; Lin, Z.; Zhao, M. Q.; Shpigel, N.; Levi, M. D.; Halim, J.; Taberna, P. L.; Barsoum, M. W.; Simon, P.; et al. Ultra-High-Rate Pseudocapacitive Energy Storage in Two-Dimensional Transition Metal Carbides. *Nat. Energy* **2017**, *6* (July), 1–6.
 - (6) Simon, P. Two-Dimensional MXene with Controlled Interlayer Spacing for Electrochemical Energy Storage. *ACS Nano* **2017**, *11* (3), 2393–2396.
 - (7) Anasori, B.; Lukatskaya, M. R.; Gogotsi, Y. 2D Metal Carbides and Nitrides (MXenes) for Energy Storage. *Nat. Rev. Mater.* **2017**, *2* (2).
 - (8) Hu, M.; Hu, T.; Li, Z.; Yang, Y.; Cheng, R.; Yang, J.; Cui, C.; Wang, X. Surface Functional Groups and Interlayer Water Determine the Electrochemical Capacitance of Ti₃C₂T_x MXene. *ACS Nano* **2018**, *12* (4), 3578–3586.
 - (9) Moitzheim, S.; De Gendt, S.; Vereecken, P. M. Investigation of the Li-Ion Insertion Mechanism for Amorphous and Anatase TiO₂ Thin-Films. *J. Electrochem. Soc.* **2019**, *166* (2), A1–A9.

- (10) Ghidui, M.; Lukatskaya, M. R.; Zhao, M. Q.; Gogotsi, Y.; Barsoum, M. W. Conductive Two-Dimensional Titanium Carbide “clay” with High Volumetric Capacitance. *Nature* **2015**, *516* (7529), 78–81.
- (11) Feng, A.; Yu, Y.; Jiang, F.; Wang, Y.; Mi, L.; Yu, Y.; Song, L. Fabrication and Thermal Stability of NH₄HF₂-Etched Ti₃C₂ MXene. *Ceram. Int.* **2017**, *43* (8), 6322–6328.
- (12) Li, M.; Lu, J.; Luo, K.; Li, Y.; Chang, K.; Chen, K.; Zhou, J.; Rosen, J.; Hultman, L.; Eklund, P.; et al. Element Replacement Approach by Reaction with Lewis Acidic Molten Salts to Synthesize Nanolaminated MAX Phases and MXenes. *J. Am. Chem. Soc.* **2019**, *141* (11), 4730–4737.
- (13) Li, Y.; Shao, H.; Lin, Z.; Lu, J.; Liu, L.; Duployer, B.; Persson, P. O. Å.; Eklund, P.; Hultman, L.; Li, M.; et al. A General Lewis Acidic Etching Route for Preparing MXenes with Enhanced Electrochemical Performance in Non-Aqueous Electrolyte. *Nat. Mater.* **2020**, *19* (8), 894–899.
- (14) Kamysbayev, V.; Filatov, A. S.; Hu, H.; Rui, X.; Lagunas, F.; Wang, D.; Klie, R. F.; Talapin, D. V. Covalent Surface Modifications and Superconductivity of Two-Dimensional Metal Carbide MXenes. *Science* (80-.). **2020**, *369* (6506), 979–983.
- (15) Li, M.; Li, X.; Qin, G.; Luo, K.; Lu, J.; Li, Y.; Liang, G.; Huang, Z.; Zhou, J.; Hultman, L.; et al. Halogenated Ti₃C₂ MXenes with Electrochemically Active Terminals for High-Performance Zinc Ion Batteries. *ACS Nano* **2021**, *15* (1), 1077–1085.
- (16) Mashtalir, O.; Naguib, M.; Mochalin, V. N.; Dall’Agnese, Y.; Heon, M.; Barsoum, M. W.; Gogotsi, Y. Intercalation and Delamination of Layered Carbides and Carbonitrides. *Nat. Commun.* **2013**, *4*, 1–7.

- (17) Alhabeab, M.; Maleski, K.; Anasori, B.; Lelyukh, P.; Clark, L.; Sin, S.; Gogotsi, Y. Guidelines for Synthesis and Processing of Two-Dimensional Titanium Carbide (Ti₃C₂T_x MXene). *Chem. Mater.* **2017**, *29* (18), 7633–7644.
- (18) Mashtalir, O.; Lukatskaya, M. R.; Zhao, M. Q.; Barsoum, M. W.; Gogotsi, Y. Amine-Assisted Delamination of Nb₂C MXene for Li-Ion Energy Storage Devices. *Adv. Mater.* **2015**, *27* (23), 3501–3506.
- (19) Naguib, M.; Unocic, R. R.; Armstrong, B. L.; Nanda, J. Large-Scale Delamination of Multi-Layers Transition Metal Carbides and Carbonitrides “MXenes.” *Dalt. Trans.* **2015**, *44* (20), 9353–9358.
- (20) Holder, C. F.; Schaak, R. E. Tutorial on Powder X-Ray Diffraction for Characterizing Nanoscale Materials. *ACS Nano* **2019**, *13* (7), 7359–7365.
- (21) Ahmed, B.; Anjum, D. H.; Hedhili, M. N.; Gogotsi, Y.; Alshareef, H. N. H₂O₂ Assisted Room Temperature Oxidation of Ti₂C MXene for Li-Ion Battery Anodes. *Nanoscale* **2016**, *8* (14), 7580–7587.
- (22) Yuen, A. C. Y.; Chen, T. B. Y.; Lin, B.; Yang, W.; Kabir, I. I.; De Cachinho Cordeiro, I. M.; Whitten, A. E.; Mata, J.; Yu, B.; Lu, H. D.; et al. Study of Structure Morphology and Layer Thickness of Ti₃C₂ MXene with Small-Angle Neutron Scattering (SANS). *Compos. Part C Open Access* **2021**, *5* (May), 100155.
- (23) Lipatov, A.; Lu, H.; Alhabeab, M.; Anasori, B.; Gruverman, A.; Gogotsi, Y.; Sinitskii, A. Elastic Properties of 2D Ti₃C₂T_x MXene Monolayers and Bilayers. *Sci. Adv.* **2018**, *4* (6), 1–8.
- (24) Birkl, C. R.; Roberts, M. R.; McTurk, E.; Bruce, P. G.; Howey, D. A. Degradation Diagnostics for Lithium Ion Cells. *J. Power Sources* **2017**, *341*, 373–386.
- (25) Kong, F.; He, X.; Liu, Q.; Qi, X.; Zheng, Y.; Wang, R.; Bai, Y. Improving the Electrochemical Properties of MXene Ti₃C₂ Multilayer for Li-Ion Batteries by Vacuum Calcination. *Electrochim. Acta* **2018**, *265*, 140–150.

- (26) Lv, G.; Wang, J.; Shi, Z.; Fan, L. Intercalation and Delamination of Two-Dimensional MXene (Ti₃C₂T_x) and Application in Sodium-Ion Batteries. *Mater. Lett.* **2018**, *219*, 45–50.
- (27) Xie, Y.; Naguib, M.; Mochalin, V. N.; Barsoum, M. W.; Gogotsi, Y.; Yu, X.; Nam, K. W.; Yang, X. Q.; Kolesnikov, A. I.; Kent, P. R. C. Role of Surface Structure on Li-Ion Energy Storage Capacity of Two-Dimensional Transition-Metal Carbides. *J. Am. Chem. Soc.* **2014**, *136* (17), 6385–6394.
- (28) Liu, L.; Lin, Z.; Chane-Ching, J. Y.; Shao, H.; Taberna, P. L.; Simon, P. 3D RGO Aerogel with Superior Electrochemical Performance for K – Ion Battery. *Energy Storage Mater.* **2019**, *19*, 306–313.
- (29) Guan, Y.; Zhang, M.; Qin, J.; Ma, X.; Li, C.; Tang, J. Hydrophilicity-Dependent Distinct Frictional Behaviors of Different Modified MXene Nanosheets. *J. Phys. Chem. C* **2020**, *124* (25), 13664–13671.
- (30) Liu, J.; Liu, Z.; Zhang, H. Bin; Chen, W.; Zhao, Z.; Wang, Q. W.; Yu, Z. Z. Ultrastrong and Highly Conductive MXene-Based Films for High-Performance Electromagnetic Interference Shielding. *Adv. Electron. Mater.* **2020**, *6* (1), 1–8.
- (31) Wang, P.; Lu, X.; Boyjoo, Y.; Wei, X.; Zhang, Y.; Guo, D.; Sun, S.; Liu, J. Pillar-Free TiO₂/Ti₃C₂ Composite with Expanded Interlayer Spacing for High-Capacity Sodium Ion Batteries. *J. Power Sources* **2020**, *451* (October 2019), 227756.
- (32) Arole, K.; Blivin, J. W.; Saha, S.; Zhao, X.; Holta, D. E.; Sarmah, A.; Cao, H.; Radovic, M.; Lutkenhaus, J. L.; Green, M. J. Water-Dispersible Ti₃C₂T_z MXene Nanosheets by Acid-Free, Molten Salt Etching. *Cell Press* **2021**, *1* (2), 35.

TOC Graphics

